

# A Practical Guide to Calculating Collision Cross Sections from Experimental Data

## 1. Overview of the MoQToF instrument

All ion mobility mass spectrometers consist of the following parts:

- An ion source
- An ion mobility drift tube
- A mass analyser
- An ion detector

Ions are most commonly transferred between these regions by electrostatic lenses. In the particular case of the MoQToF (figs.1,2) (McCullough *et al.* 2008) ions are produced by electrospray or nano-electrospray ionisation; they pass through two skimmers (cone and extractor) before they enter the region of the first RF hexapole H1. Ions are trapped in H1 by the oscillating RF voltage of the hexapole and the repulsive potentials on the extractor and the top hat lens 1 (TH1) which are situated on either end of H1. Ions are accumulated in the trapping region for 200 ToF 'pushes'. At  $t_0$  of an IM experiment a square pulse (the width of which is less than  $50\mu\text{s}$ , typically ranging between 25 and  $45\mu\text{s}$ ) of ions is injected into the drift cell. The ion pulse is first focused and steered by three lens elements (L1, L2, L3) into the entrance of the drift tube, where they drift under the influence of a weak electric field and then, upon exit are re-focused by L4 and enter the second hexapole H2. From there the ions are guided through the quadrupole analyser and the collision cell before they are steered into the ToF region. A high-voltage pulse pushes the ions down the orthogonally situated ToF. The IM 'clock' stops at that point, limiting the time resolution to  $t_{\text{push}}$ . The ions then drift in the ToF, are reflected and then detected by the MCPs.

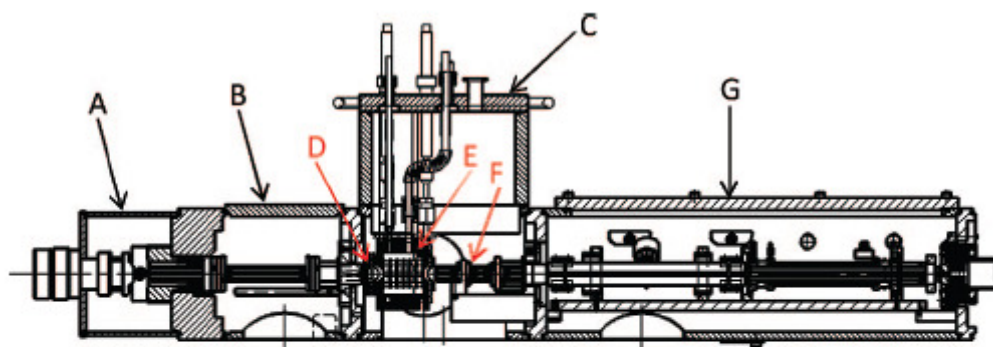


**Figure 1.** Schematic diagram of the MoQToF. (A) z-Spray ESI ion source; (B) vacuum chamber 1 housing precell hexapole; (C) vacuum chamber 2, new chamber housing the precell Einzel lens (D); drift cell (E); and postcell hexapole (F); this chamber also contains all gas and electric feedthroughs for the drift cell; (G) vacuum chamber 3 housing the quadrupole mass analyzer and hexapole collision cell leading to the orthogonal ToF mass analyzer (not shown).

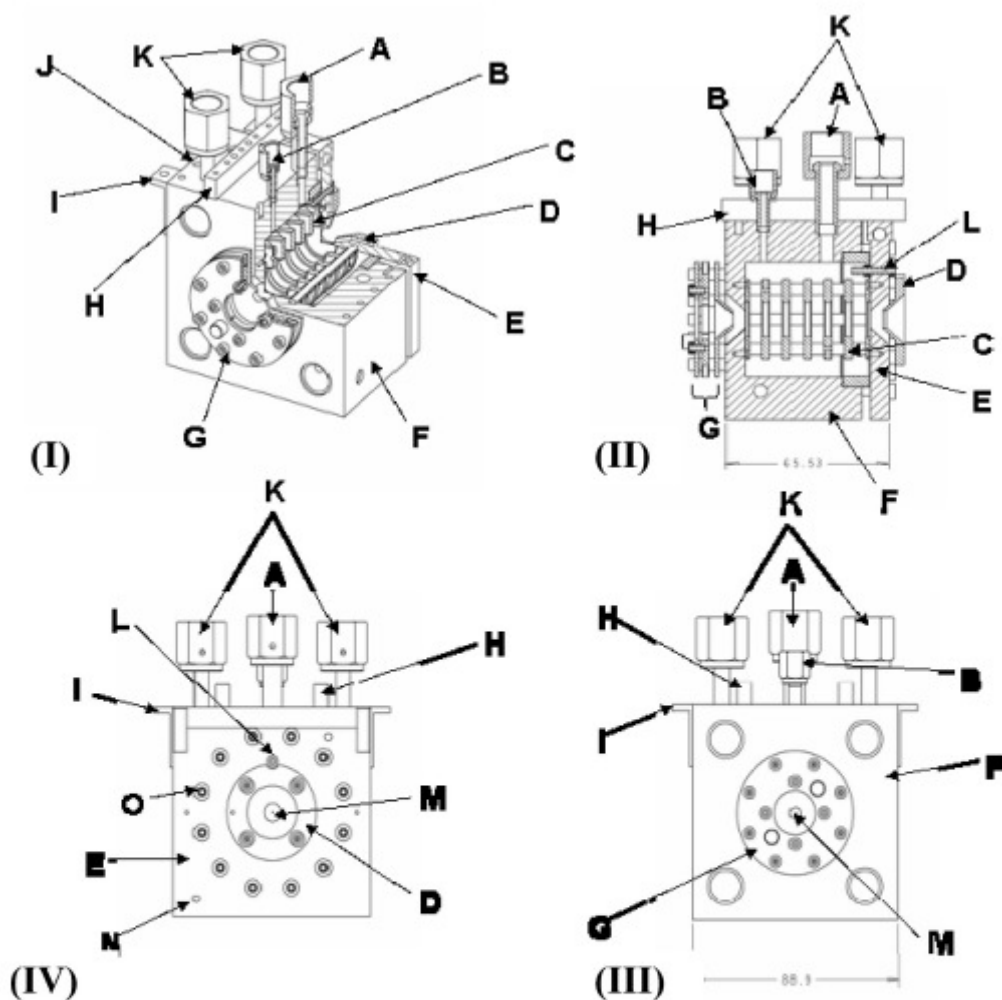


**Figure 2.** Cell drawings for the MoQToF drift cell. (I) 3D section through cell; (II) section through cell viewed from side; (III) front elevation; (IV) rear elevation. Parts are labeled as follows: (A) baratron connection; (B) gas in; (C) drift rings; (D) exit lens (L4); (E) end cap (C2); (F) cell body (C1); (G) Einzel lens (L1, L2, and L3); (H) heater terminal block; (I) mounting brackets; (J) heaters; (K) cooling line inlets; (L) feedthrough to drift rings; (M) molybdenum orifice; (N) thermocouple mounting; (O) cell screws.

## 2. Theoretical background

Thus the measured arrival time corresponds to the time ions spend between TH1 and the ToF pusher. This time,  $t_a$  can be thought of as a sum of the drift time  $t_D$  and the time the ions spend outside the drift tube  $t_0$  – the latter being thought of as independent of the drift voltage:

$$t_a = t_D + t_0 \quad \{1\}$$

Now, at low electric fields the drift velocity  $v_D$  is directly proportional to the electric field  $E$ , the mobility being independent of the electric field; thus an expression for  $t_D$  can be obtained:

$$v_D = K\mathbf{E} \Rightarrow \frac{z_D}{t_D} = K \frac{V_D}{z_D} \Rightarrow t_D = \frac{z_D^2}{KV_D} \quad \{2\}$$

Where  $K$  is the mobility,  $E$  the drift electric field,  $V_D$  the drift voltage and  $z_D$  the longitudinal drift distance *i.e.* the distance between the entrance and exit apertures of the drift tube. Substituting {2} into {1} and differentiating with respect to  $(V_D)^{-1}$  we obtain a direct relation between the average arrival time and the low-field mobility independent of  $t_0$  under the condition that  $t_0$  does not vary with  $V_D$ :

$$\frac{dt_a}{d\left(\frac{1}{V_D}\right)} = \frac{z_D^2}{K} \quad \{3\}$$

In order to account for fluctuations in the pressure ( $P$ ) and temperature ( $T$ ) of the buffer gas, but also to facilitate comparison with literature values, we define the *reduced mobility* as

$$K^\circ = K \frac{T^\circ}{T} \frac{P}{P^\circ} \quad \{4\}$$

where  $T^\circ$  and  $P^\circ$  signify standard temperature and pressure, respectively. Thus substituting into {2} and using {1} we derive our final expressions:

$$t_a = \frac{z_D^2 T^\circ}{K^\circ T P^\circ} \frac{P}{V_D} + t_0 \quad \{5\}$$

$$K^\circ = \frac{z_D^2 T^\circ}{P^\circ T \left( \frac{dt_a}{d\left(\frac{P}{V_D}\right)} \right)} \quad \{6\}$$

Note that this time we chose to differentiate against  $P/V_D$  in order to associate each particular pressure reading with its corresponding drift voltage. That ratio is also inversely proportional to the field strength  $E/N$  by a factor of  $k_B T/z_D$ . ( $N$  being the buffer gas number density). This method requires measurements at different drift

voltages; yet this is not entirely undesirable since it can serve as an internal control of the experiment's validity; for only at low fields is the relationship between  $t_a$  and  $P/V_D$  (i.e. drift velocity and  $E/N$ ) linear.

Using kinetic theory, the mobility at low fields can be related to the momentum transfer cross section  $\Omega$  via:

$$K = \frac{3}{16} \frac{q}{N} \left( \frac{2\pi}{\mu k_B T} \right)^{1/2} \frac{1}{\Omega} \quad \{7\}$$

We shall now proceed with a practical example for the analysis of an IMMS experiment of Bradykinin.

### 3. Analysis of experimental data

When the MoQToF is used in ion mobility mode, the data we obtain for a species of a particular  $m/z$  at a specific  $V_D$  looks like the chromatogram displayed in figure 3.

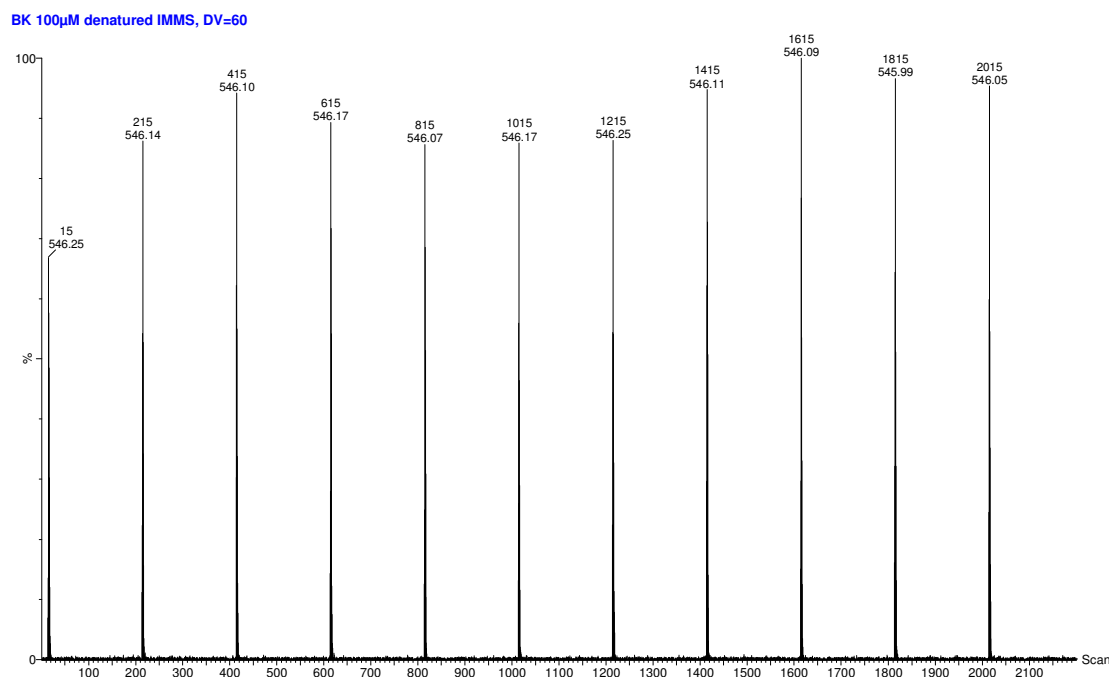


**figure 3.** masslynx data for the 2+ charge state of bradykinin at a drift voltage of 50V

Essentially, this represents several repetitions of an ion mobility measurement, each having a duration of *ca.* 25 seconds. The maximum drift time recorded is 200 scans, each scan having the duration of one ToF pusher period (which is of the order of 100 $\mu$ s). Some of the benefits inherent of this method are that the ion intensity can be monitored during the experiment and occasionally the convergence of the experimental arrival time distribution (ATD) can be monitored. Datasets like this of fig.3 must be cropped and summed to obtain an average ATD like the one of fig.4.

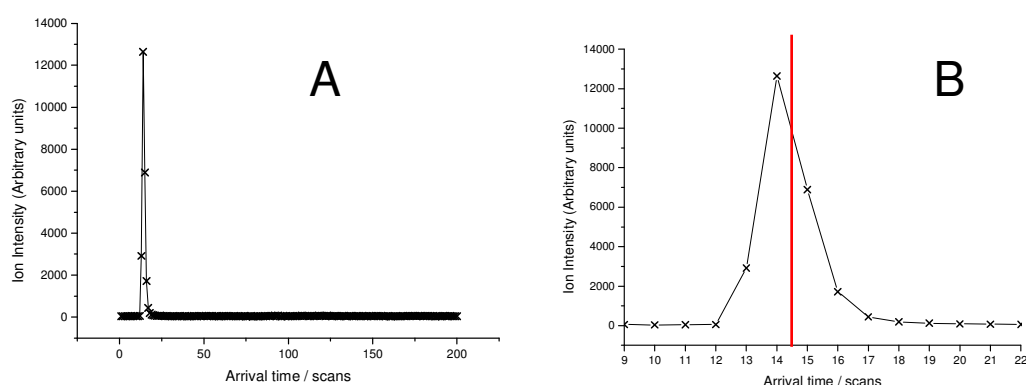


**figure 4.** Average ATD obtained for BK<sup>2+</sup> at 60V. B; zoomed in view of A – the points have been connected by lines in order to guide the eye. The red line shows the average scan obtained, 14.437 scans = 1010.59 $\mu$ s. This ATD was summed from 10 identical experiments each lasting 25 seconds with a pusher period of 70 $\mu$ s; i.e. it corresponds to  $10 \lfloor (25/7 \cdot 10^{-5}) - 1 \rfloor = 3571410$  ion pulses.

Assuming that the most significant features of the ATD exist between the detector's range, the ion intensity can be easily conceived as being directly proportional to the population of ion species that exit the drift tube and are transferred successfully to the MCPs. For our analysis we seek an estimate of the average time. Such a quantity (as well as any other time depended function) can be calculated directly from the experimental ATD:

$$\bar{t}_{a,v_b} = \frac{\sum I(t)}{\sum I(t)} \quad \{9\}$$

This method will yield the *average* arrival time of all species included in a particular peak of the mass spectrum; if several partially resolved conformers are present, fitting the ATD to a function is necessary in order to obtain more meaningful data. An outline of the calculations needed to obtain a distribution descriptive of the experiment as well as a number of useful solutions will be given in the next section.

If the background noise levels are appreciable, a background subtraction of the average ATD may be useful before the averaging procedure. ToF MS scans can be easily converted to time by multiplying the scan number by the ToF pusher time. Furthermore, scans where the ion signal intensity is similar to the noise levels may be avoided, in order to prevent spurious signal from influencing our estimate of the arrival time.

The above process may be repeated for all voltages measured, thus yielding a list of average arrival times vs.  $P/V$  (Table I; figure 5).

TABLE I

<u>P/torr</u>	<u>P/V</u>	<u>Drift Voltage</u>	<u>Arrival Time</u> <u>(<math>\mu</math>s)</u>
2.994	0.059760479	50.1	1077.481107
3.006	0.07515	40	1180.726789
3.015	0.086142857	35	1243.608214
3.014	0.100466667	30	1341.623022
3.015	0.1206	25	1479.979536
3.001	0.15005	20	1672.295942

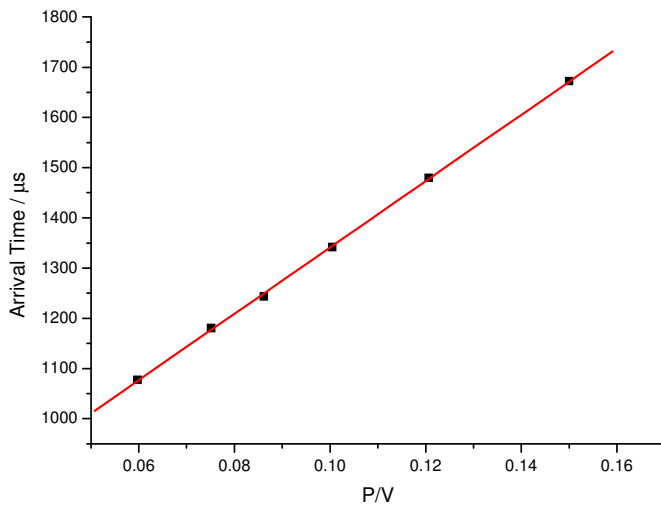
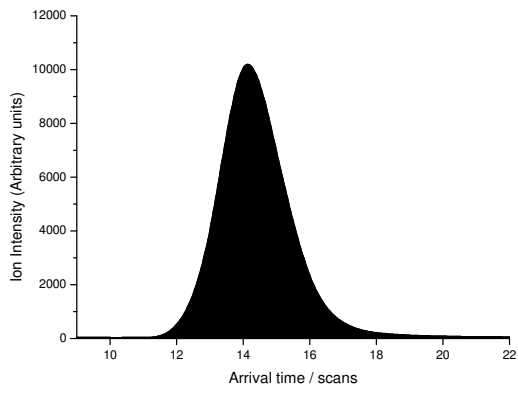


*figure 5.* Plot of arrival time vs.  $P/V$  for the 2+ BK ion

As expected, the arrival time does increase with increasing  $P/V$  and the relationship is linear as far as we can see, indicating that we are still within the low-field regime. The intercept at the time axis ( $\approx 681\mu\text{s}$ ) corresponds to the ‘dead’ time, i.e. the time the ions spend in the instrument if no drift had taken place, and the slope (6603.3) can be used to calculate the mobility and cross section from {6} and {7}. These were found to be  $4.691 \text{ cm}^2/\text{Vs}$  and  $227.4 \text{ \AA}^2$  respectively.



#### 4. A primer on mathematical modelling of the ATD

Conformational fluctuations in gas-phase peptides can be roughly divided into three categories according to their timescales:

- a) Fast transitions or interconversions ( $\tau \ll t_{obs}$ )
- b) Transitions of intermediate speed ( $\tau \approx t_{obs}$ )
- c) Slow transitions ( $\tau \gg t_{obs}$ )

Conformers that either undergo fast interconversion or have very similar mobilities will yield single, unresolvable peaks in an arrival time spectrum; for such species only average cross-sections of all species can be obtained. The analysis of arrival time distributions for ions undergoing processes at a timescale similar to that of the experiment (i.e. milliseconds) will depend on the specific system and experiment in question, but a more detailed kinetic model may be called for. Conformers with significantly different mobilities that do not interconvert, or do so very slowly, will give rise to resolved ATDs; it is often the case however that the resolution is not sufficient to accurately calculate an average drift time directly. In such cases fitting to an analytical solution of the ion current as a function of time while adjusting all other parameters to agree with the experimental setup is necessary. In order to do this, a mathematical model for describing the drift of ions in drift tubes is needed. Much work to this end has already been done in the 1950s, 60s and 70s; a list of relevant references is given by Mason & McDaniel (1973, pp. 86-93) and a dense extensive discussion on the quantification of many effects relevant to such experiments has been written by Gatland (1974). Here we only review the very basic steps that are common in deriving an appropriate expression for IM experiments at low fields.

Ions drifting in an IM experiment can be thought to undergo two processes. First, thermal motion, i.e. a random walk in space, leading to diffusion. An account of diffusion in terms of the ion flux (current)  $\mathbf{J}$ , is given by Fick's first law of diffusion:

$$\mathbf{J} = -D\nabla N \quad \{10\}$$

The second phenomenon is the directed motion of all ions along the direction of the applied field

$$\mathbf{J} \propto v_D N \quad \{11\}$$

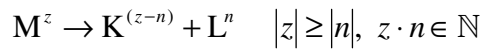
Combining {10} {11} and {2} we obtain

$$\mathbf{J} = K\mathbf{E}N - D\nabla N \quad \{12\}$$

The time evolution of the ion density  $N$  is given by

$$\frac{\partial N}{\partial t} = -\nabla \cdot \mathbf{J} = \nabla D \nabla N - K\mathbf{E} \cdot \nabla N \quad \{13\}$$

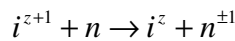
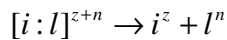
Further terms may be added to this expression rendering it more accurate. For instance, ions may undergo depleting reactions with neutrals; in terms of protein and peptide ions, gas-phase collisionally induced fragmentation is one such process occurring between the analyte ions and the buffer gas:



Such depleting processes for an ion  $i$  will happen proportionally to  $N_i$  and given the sum of all depleting reaction frequencies to be  $\alpha_-$  the transport equation {13} for species  $i$  becomes

$$\frac{\partial N_i}{\partial t} = \nabla D \nabla N_i - K E \nabla N_i - \alpha_- N_i \quad \{14\}$$

In addition to processes depleting reactions, processes that produce the analyte species may take place. Dissociation of a non-covalent complex to retrieve the analyte ion or charge transfer are illustrative of such processes:



Any process of the type  $j \xrightarrow{\alpha_{ij}} i$  where  $\alpha_{ij}$  is the reaction frequency will contribute to the ion density; such effects may be formulated mathematically as

$$\frac{\partial N_i}{\partial t} = \nabla D_i \nabla N_i - K_i E \nabla N_i - \alpha_- N_i + \sum_j \alpha_{ij} N_j \quad \{15\}$$

One may argue that the contribution of reactions to the particular population of ions of a certain  $m/z$  as they drift at low fields is negligible; however different geometries of the same macromolecular ion will be characterised by a different diffusion coefficient and mobility, so that the interconversion between different conformers can also be described by {15}; such effects are of primary interest in IMMS experiments of biomacromolecular ions.

Expressions like the ones described above can be solved using the Green's function method, which is generally applicable to problems of the form  $\mathfrak{L}f(x) = s(x)$  (here for simplicity only shown in one dimension,  $x$ ) where  $\mathfrak{L}$  is a linear operator. We seek a function  $G(x, x')$  with the property  $\mathfrak{L}G(x, x') = \delta(x - x')$  where  $\delta$  is the Dirac delta function and  $x'$  the source point, yielding the solution  $f(x) = \int G(x, x')s(x')dx'$ . An interesting property of such solutions is that any number functions  $g(x)$  that satisfy  $\mathfrak{L}g(x) = 0$  can be added to the original Green's function, allowing for the construction of an expression that accounts for several other properties of the ion swarm, such as boundary conditions.

Now, in the case of {14}, the operator  $\mathfrak{L}$  is given by

$$\mathfrak{L} = \frac{\partial}{\partial t} - D\nabla^2 + KE\nabla + \alpha_+ \quad \{16\}$$

The Green's function corresponding to this problem is known:

$$G(\mathbf{r}, \mathbf{r}', t, t') = \frac{e^{-\frac{x^2+y^2+(z-v_D t)^2}{4Dt} - \alpha_+ t}}{(4\pi Dt)^{3/2}} \quad \{17\}$$

Thus the estimation of the ion density is possible:

$$N(\mathbf{r}, t) = \int G(\mathbf{r}, \mathbf{r}', t, t') s(\mathbf{r}', t') d\mathbf{r}' dt' \quad \{18\}$$

the function  $s(\mathbf{r}', t')$  is the initial condition and in the context of our experiments is interpreted as the distribution of ions as they enter the drift region; moreover, it can be adjusted to mirror the appropriate initial ion distribution. Barnes (1967) provides solutions for  $N(\mathbf{r}, t)$  for different ion sources and initial ion distributions. Here we reproduce the 1-dimensional solution obtained with an initial delta, square pulse and Gaussian distribution ( $n_0$  is the initial number of ions entering the drift tube):

1. Dirac delta initial ion distribution

$$s(z) = n_0 \delta(z) \quad \{19\}$$

$$N(z, t) = \frac{n_0 e^{-\frac{(z-v_D t)^2}{4Dt} - \alpha_+ t}}{(4\pi Dt)^{1/2}} \quad \{20\}$$

2. Square pulse initial ion distribution

$$s(z) = \frac{n_0}{2w} \quad -w \leq z \leq w \quad \{21\}$$

$$s(z) = 0 \quad z < -w, \quad z > w$$

$$N(z, t) = \frac{n_0 e^{-\alpha_+ t}}{2w} \left[ \operatorname{erf} \left( \frac{z+w-v_D t}{(4Dt)^{1/2}} \right) - \operatorname{erf} \left( \frac{z-w-v_D t}{(4Dt)^{1/2}} \right) \right] \quad \{22\}$$

3. Gaussian initial ion distribution

$$s(z) = \frac{n_0}{(2\pi\sigma^2)^{1/2}} e^{-\frac{z^2}{2\sigma^2}} \quad \{23\}$$

$$N(z, t) = \frac{n_0 e^{-\frac{(z-v_D t)^2}{2\sigma^2+4Dt} - \alpha_+ t}}{[2\pi(\sigma^2 - Dt)]^{1/2}} \quad \{24\}$$

Another interesting solution is described by Moseley *et al.* (1969); the analysis delineated therein attempts at a treatment of the ion density distribution at high fields

as well rendering a necessary distinction between diffusion along directions parallel and perpendicular to the axis of the applied field. Thus,  $\mathfrak{L}$  is expressed as:

$$\mathfrak{L} = \frac{\partial}{\partial t} - D_T \left( \frac{\partial^2}{\partial x^2} + \frac{\partial^2}{\partial y^2} \right) - D_L \frac{\partial^2}{\partial z^2} + v_D \frac{\partial}{\partial z} + \alpha_- \quad \{25\}$$

where  $D_T$  and  $D_L$  are the transverse and longitudinal diffusion coefficients, respectively. Furthermore, the source term is given by:

$$s(\mathbf{r}', t') = \frac{b}{\pi r_0^2} H(r_0 - r') \delta(z') \delta(t) \quad \{26\}$$

an expression describing “an axially thin disk source of  $b$  ions with uniform surface density and radius  $r_0$ , being created instantaneously at  $t' = 0$  in the plane  $z' = 0$ .”  $H(x)$  is a step function whereby  $H(x < 0) = 0$  and  $H(x \geq 0) = 1$ . The authors thus arrive at a solution describing the ion density at every point in space and time from which an expression for the axial ion density can be derived which, interestingly, depends on both longitudinal and transverse diffusion coefficients:

$$N(z, t) = \frac{b}{4\pi r_0^2 (\pi D_L t)^{\frac{1}{2}}} e^{-\frac{(z-v_D t)^2}{4D_L t} - \alpha_- t} \left( 1 - e^{-\frac{r_0^2}{4D_T t}} \right) \quad \{27\}$$

Recalculating the ion flux from {27} using {12} one obtains

$$\Phi(z, t) = \frac{A}{4(\pi D_L t)^{\frac{1}{2}}} \left( v_D + \frac{z}{t} \right) e^{-\frac{(z-v_D t)^2}{4D_L t} - \alpha_- t} \left( 1 - e^{-\frac{r_0^2}{4D_T t}} \right) \quad \{28\}$$

$\Phi(z, t)$  describes the flux of ions from the exit aperture at the  $z$  axis using {26} as the initial ion distribution.  $A$  is a measurement-dependent constant representing the total number of ions reaching the detector and depends on the size of the entrance and exit apertures as well as the number of ions which enter the drift tube; in the case of the MoQToF it can be taken to also represent the transmission efficiency of ions through the remaining parts of the instrument until they enter the ToF drift region, assuming that the ion density is not itself perturbed by those parts.

In summary, motion of ions in a drift tube is determined by the applied field and the mobility of the ionic species. Such a drift will result to a certain asymmetry in the ionic density distribution for a number of reasons:

- Since the space the ion swarm occupies is of the same order of magnitude as the drift length, ions in the beginning of the distribution will have undergone less diffusion than the ones at the tail
- {At high fields} the longitudinal and transverse diffusion coefficients are not identical
- During their drift, analyte ions may undergo depleting or forming processes that further complicate the shape of the ATD. Again ions drifting for a longer time will be subjected to more reactions than those arriving earlier at the exit aperture
- In addition to the above, end effects (caused by the injection of ions into the drift region as well as the rushing of buffer gas out of the drift cell close to the apertures) which are not quantified here may contribute to the asymmetry of the ATD.

Thus it's clear that simply fitting an ATD to a symmetrical distribution is likely to cause erroneous estimates of experimental observables. Instead, equations {20}, {22}, {24} and {27} can provide the basis for the fitting. When multiple ATDs are present in the same spectrum, a sum of several functions of a form similar to {28} can be used to construct a curve that fits the experimental data. Of course, at low fields  $D_L \approx D_T$ ,  $D \approx K \frac{k_B T}{q}$  and  $v_D = KE$ , thus when fitting {28} to experimental ATDs,

all 'unknown' quantities can be expressed in terms of the drift velocity, the only parameters that need to be determined being the drift velocity, the total number of ions, the background noise (the latter two are entirely dependent on specific measurements) and, finally, the number of species that are suspected to be contained within the experimental ATD.

Happy Analysing!

## 5. References

**Barnes W.S.** Method of Analysis of Ion Swarm Experiments (1967) *Phys. Fluids* 10:1941

**Gatland I.R.** Analysis for Ion Drift Tube Experiments (1974) *Case Stud. Atom. Phys.* 4:369

**McDaniel E.W. and Mason E.A.** The Mobility and Diffusion of Ions in Gases (1973) *Wiley, NY*

**McCullough B.J., Kalapothakis J.M.K., Eastwood H.L., Kemper P., MacMillan D., Taylor K., Dorin J. and Perdita E. Barran** Development of an Ion Mobility Quadrupole Time of Flight Mass Spectrometer (2008) *Anal. Chem.* (in press)

**Moseley J.T., Gatland I.R., Martin D.W. and McDaniel E.W.** Measurement of Transport Properties of Ions in Gases: Results for  $K^+$  ions in  $N_2$  (1969) *Phys. Rev.* 178:234

**Wannier G.H.** On the Motion of Gaseous Ions in a Strong Electric Field I (1941) *Phys. Rev.* 83:281

**Wannier G.H.** On the Motion of Gaseous Ions in a Strong Electric Field II (1952) *Phys. Rev.* 87:795

The Bowers group website at UCSB also contains a good synoptic overview of some topics discussed herein:  
[http://bowers.chem.ucsb.edu/theory\\_analysis/index.shtml](http://bowers.chem.ucsb.edu/theory_analysis/index.shtml)